Superscars in Billiards: A Model for Doorway States in Quantum Spectra

S. Åberg,[1] T. Guhr,[1,2] M. Miski-Oglu,[3] and A. Richter[3]
[1]*Matematisk Fysik, LTH, Lunds Universitet, Box 118, 22100 Lund, Sweden*
[2]*Fachbereich Physik, Universität Duisburg-Essen, Lotharstrasse 1, 47057 Duisburg, Germany*
[3]*Institut für Kernphysik, Technische Universität Darmstadt, Schlossgartenstrasse 9, Darmstadt, Germany*
(Received 27 November 2007; published 23 May 2008)

In a unifying way, the doorway mechanism explains spectral properties in a rich variety of open mesoscopic quantum systems, ranging from atoms to nuclei. A distinct state and a background of other states couple to each other which sensitively affects the strength function. The recently measured superscars in the barrier billiard provide an ideal model for an in-depth investigation of this mechanism. We introduce two new statistical observables: the full distribution of the maximum coupling coefficient to the doorway and directed spatial correlators. Using random matrix theory and random plane waves, we obtain a consistent understanding of the experimental data.

DOI: 10.1103/PhysRevLett.100.204101 PACS numbers: 05.45.Mt, 03.65.Sq, 24.30.Cz

Strength function phenomena [1] in open mesoscopic quantum systems are a central object of study in atomic and molecular physics as well as in atomic clusters, quantum dots, and in nuclear physics. Often there is a somehow ''distinct'' and ''simple'' excitation whose amplitude is spread over many ''complicated'' states. The distinct state thus acts as a ''doorway'' to the (usually chaotic) background of the complicated states [1,2]. Prime examples are isobaric analog states and multipole giant resonances (GR) in nuclear physics. The strength function is typically of Breit-Wigner (BW) shape with a characteristic spreading width [3–6]. For examples from molecules and metal clusters, see [7–9].

Quantum billiards can be realized experimentally by flat microwave resonators [10]. To study the doorway mechanism in detail, we use a microwave billiard of rectangular shape with a thin barrier inside; see Fig. 1. The electric field strength distribution corresponding to the quantum wave function is reconstructed from the measured intensities. Certain wave functions of this pseudointegrable billiard possess unique structures called ''superscars'' [11,12]. These are scarring wave functions related to families of neutrally stable classical periodic orbits. Four examples of measured superscars are shown in Fig. 1. Unlike ordinary scars [13], which are localized around a single unstable periodic orbit, they do not disappear at large quantum numbers. They are embedded into, but clearly distinct from, a large number of nonscarred wave functions. We will demonstrate that the superscars act as doorways to the background of the nonscarred wave functions. Our perfect control over the experimental observables allows us an in-depth study of the doorway mechanism which can presently not be accomplished in traditional quantum systems.

First, we briefly compile the necessary information on measured superscars in the barrier billiard. Second, we introduce the maximal coupling coefficient as a new observable and use random matrix theory (RMT) [14] to model its distribution. Third, we introduce directed spatial correlators as another new observable and model them by extending Berry's random wave ansatz [15].

As Fig. 1 shows, the superscars with a clear wave function structure relate to particular classical periodic orbits. The superscars form a family which lives within an infinitely long periodic orbit channel (POC). Because of diffraction on the tip of the barrier, the amplitude of the scarred wave function tends to zero along the POC boundary. Thus, the superscarred wave function can be approximated by a constructed superscar state, defined as an eigenfunction $\Psi^{(\mathsf{F})}_{m,n}(\vec{r})$ in the infinitely long POC [11,12]. Here $\mathsf{F} \in \{\mathsf{BB}, \mathsf{V}, \mathsf{D}, \mathsf{W}\}$ stands for the superscar families (BB: bouncing ball; V: inverted; D: diamond; W), see Fig. 1, and (m, n) are the numbers of wave maxima along and perpendicular to the POC. A measured state $\Psi_{\tilde{f}}(\vec{r})$ at (rescaled) frequency $\tilde{f}$ in the barrier billiard has an overlap,

$$c_{m,n} = \langle \Psi^{(\mathsf{F})}_{m,n} | \Psi_{\tilde{f}} \rangle, \tag{1}$$

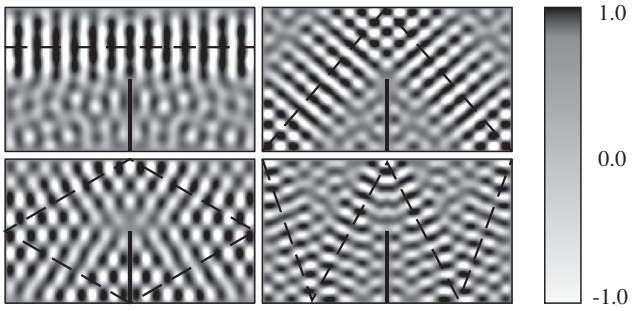

FIG. 1. Examples for measured superscars induced by the barrier and concentrated along the indicated classical periodic orbits (dashed lines). They are members of four different families. Top row: horizontal bouncing ball BB and inverted V superscars; bottom row: diamond D and W superscars. The gray level indicates the value of the wave function (black: highest positive, white: most negative value; see [12]).

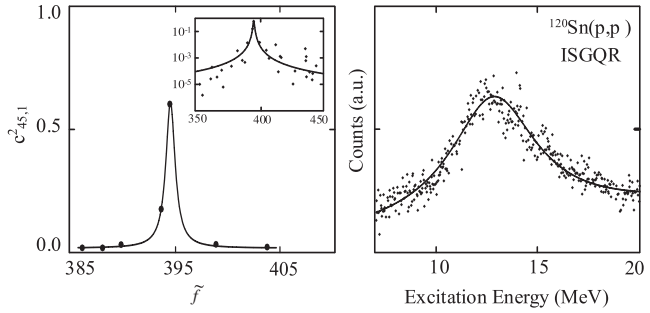

FIG. 2. Doorway strength functions. Left: Overlap between constructed superscar state of the V family with $m = 45$, $n = 1$ and the measured wave functions versus rescaled frequency. The solid curve is a BW function. The inset shows the overlap on a logarithmic scale over a large frequency interval. Right: Spectrum of the (p, p') reaction at 200 MeV on ^{120}Sn in the region of the isoscalar giant quadrupole resonance (ISGQR) as an example for a nuclear doorway state [6]. The solid curve is a BW function fitted to the data.

with the constructed superscars [11,12]. As an example, the distribution of the overlaps with a constructed V superscar state with quantum numbers $(m, n) = (45, 1)$ is depicted in Fig. 2. The superscar strength spreads into neighboring nonscarring background states following a BW shape with the main strength concentrated in a few states. This nicely confirms our doorway interpretation. For comparison, a nuclear GR doorway is also plotted in Fig. 2. Here, the number of background states—reflected in the fluctuations around its BW shape—is much larger than in the barrier billiard. According to the Brink-Axel hypothesis [16,17] a GR excitation builds upon every nuclear state. Similarly, a superscar doorway state exists for each value of F, m, and n.

We now set up a random matrix model in the spirit of models in nuclear physics [1,14]. The total Hamiltonian reads $\hat{H} = \hat{H}_s + \hat{H}_b + \hat{V}$. Here, $\hat{H}_s$ and $\hat{H}_b$ describe doorway states and background states, respectively, and $\hat{V}$ couples the two classes of states. The eigenequations for the uncoupled Hamiltonians are $\hat{H}_s|s\rangle = e_s|s\rangle$ and $\hat{H}_b|b\rangle = e_b|b\rangle$. For the matrix elements of the interaction, we make the assumptions $\langle s|\hat{V}|s'\rangle = \langle b|\hat{V}|b'\rangle = 0$ and $\langle b|\hat{V}|s\rangle = v_{bs}$ for any s, s', b, b'. We interpret the constructed superscars, $\Psi^{(\mathsf{F})}_{m,n}(\vec{r})$ for a given family F but with different (m, n) as the doorway states s. Because of the interaction $\hat{V}$ the doorway state is not an eigenstate of the Hamiltonian $\hat{H}$. We assume that the interaction matrix elements, $v_{bs} = v_{sb}$, are Gaussian distributed random variables with zero mean and variance v^2. Importantly, the parameter governing the physics is v/d, where d is the mean level spacing of the background states [1,14]. Since only a few states carry superscar strength with given values of (m, n), and superscar states with different (m, n) are assumed to not mix, it is sufficient to consider only *one* superscar state s coupled to N background states b, where N is large. To resemble the experiment, we include $N = 294$ background states. As the barrier billiard is pseudointegrable, the spacings between the eigenstates are semi-Poisson distributed [18]. We thus generate such an ensemble of $N + 1$ states. The doorway state is chosen as the middle state and interacts with the surrounding N states. For each realization, energies and wave functions are numerically obtained, and the mixture of the superscar with the surrounding states is calculated. We then extract v/d for each superscar family. The full problem $\hat{H}|n\rangle = E_n|n\rangle$ is solved by the exact implicit equation

$$E_n = e_s - \sum_{b=1}^{N} \frac{v_{bs}^2}{e_b - E_n}, \tag{2}$$

and the wave functions are given by

$$|n\rangle = c_s\left(|s\rangle - \sum_{b=1}^{N} \frac{v_{bs}}{e_b - E_n}|b\rangle\right). \tag{3}$$

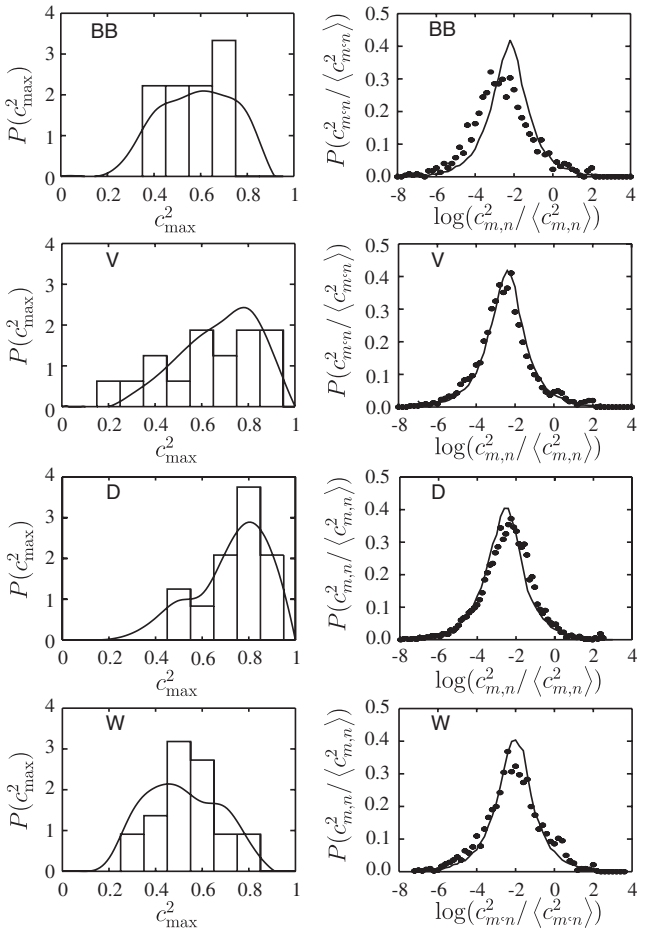

FIG. 3. Left: $c^2_{\max}$ distributions of measured superscars (histogram), and the fit of the RMT model predictions (solid line). Right: Normalized distributions of superscar strength spread over all states on a logarithmic scale. Experimental distributions (dots) are compared with the RMT model predictions.

The superscar coupling of each eigenstate is therefore

$$c_s(n) = \left(1 + \sum_{b=1}^{N} \frac{v_{bs}^2}{(e_b - E_n)^2}\right)^{-1/2}. \quad (4)$$

The superscar strength c_s^2 over the different eigenstates $|n\rangle$ is BW distributed [1] with spreading width $\Gamma^{\downarrow} = 2\pi v^2/d$, i.e., $\Gamma^{\downarrow}/d = 2\pi(v/d)^2$.

As the superscar strength is distributed over a small number of states only (see Fig. 2), v/d is smaller than or of the order of unity. The fit with a BW distribution shows a rather large variation of the fitted shape as well as the width of the distribution over the ensemble of observed superscars in a superscar family F. Hence, the width $\Gamma^{\downarrow}$ is not a well-suited measure to determine v/d. We thus consider the state with the largest coupling

$$c_{\max}^2 = \max(c_{m,n}^2) \quad (5)$$

for a given superscar which is directly obtained from experiment. Since a rather small number of states carry strength from the doorway state (i.e., the constructed superscar), the peak of the fitted BW-shaped strength function usually deviates from the measured largest superscar strength: The discretely measured state does not appear exactly at the peak. We may, however, directly compare the maximal measured value to the corresponding calculated value, $\max(c_s^2(n))$, where c_s is obtained from Eq. (4). Not only the average value of $c_{\max}^2$ can be studied but also its higher moments. We study the *full distribution* of these maximal couplings for a superscar family F, which, as far as we know, has never been considered before. In Ref. [19] the first two moments of the $c_{\max}^2$ distribution were studied, but with assumptions not valid in our context. The shape of the $c_{\max}^2$ distribution strongly depends on the interaction strength, v/d, and it is a particularly sensitive measure for small values of v/d, i.e., of the order of 1 or smaller.

In Fig. 3 we show measured distributions of $c_{\max}^2$ with the best fit curves of the RMT model for each superscar family F. The fit gives the following values for the interaction strength: for the BB superscar $v/d = 0.45$, for the V superscar $v/d = 0.35$, for the D superscar $v/d = 0.3$, and for the W superscar $v/d = 0.55$. The coupling strengths are small and thus our ansatz for a BW shape for the doorway strength function (Fig. 2) is in accordance with earlier findings [20]. The V, D, W superscar families contain 16, 25, and 22 measured members, respectively, while the BB superscar family contains only 9. The fit in this latter case has thus higher uncertainty. The average measured and calculated $c_{\max}^2$ values are listed in Table I.

Another observable is the distribution of the superscar couplings over all eigenstates. The strength of each constructed superscar is measured (and calculated) over all 294 states, where the major part of the strength is concentrated in a few states only. Figure 3 shows measured distributions compared to calculations for different interaction strengths obtained from the fit to the $c_{\max}^2$ distributions. Once more, we clearly see that the model reproduces the experimental distributions for all superscar families well except in the case of the BB superscar family because of the small number of superscars.

TABLE I. Experimental (Expt) results with standard errors of the mean versus results from RMT model and directed correlators (Corr) for averaged $c_{\max}^2$ values and spreading width $\Gamma^{\downarrow}$.

	$\langle c_{\max}^2 \rangle$			$\Gamma^{\downarrow}$	
F	Expt	RMT	Corr	Expt	RMT
BB	0.58 ± 0.05	0.58	0.81	0.9 ± 0.1	1.3
V	0.63 ± 0.05	0.68	0.69	0.8 ± 0.1	0.8
D	0.74 ± 0.03	0.72	0.69	0.9 ± 0.1	0.6
W	0.54 ± 0.03	0.51	0.49	1.0 ± 0.1	1.9

We now turn to the spatial correlations of the wave functions. Berry [15] introduced the correlator

$$C(kr) = \frac{\langle \psi_k(\vec{R} - \vec{r}/2)\psi_k^*(\vec{R} + \vec{r}/2)\rangle}{\langle |\psi_k(\vec{R})|^2\rangle} \quad (6)$$

of the wave functions $\psi_k(\vec{r})$ where the average is performed *isotropically* over all vectors $\vec{R}$ and, for fixed moduli of wave vector $\vec{k}$ and r, over all directions of the vector $\vec{r}$. In our context, all wave functions are real and no complex conjugation is needed in the definition (6). Berry argued that the spatial correlations of a wave function in an ergodic system should be indistinguishable from those of superimposed plane waves. In two dimensions this yields the universal prediction $C(kr) = J_0(kr)$, if possible boundary effects are ignored. Here J_0 is the Bessel function of

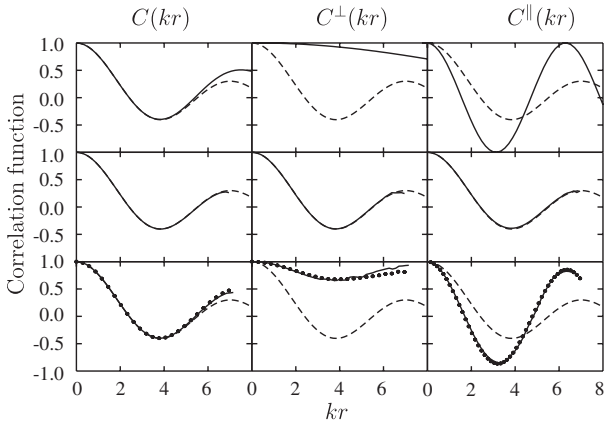

FIG. 4. The wave function correlators. The $J_0(kr)$ prediction is always given as dashed line. The top row shows the correlation function of the constructed V superscar state as solid lines: the isotropic $C(kr)$ as well as the directed $C^{\perp}(kr)$ and $C^{\parallel}(kr)$. In the middle row, the same observables are depicted as solid lines for the averages over all experimental wave functions in the barrier billiard. In the bottom row, the correlators averaged over all observed V superscars are displayed as solid lines and the correlators resulting from Eq. (7) with $c_{\max}^2 = 0.69$ are shown as filled circles.

order zero. Indeed, this behavior was confirmed in numerous systems [10,14,21,22].

The superscars, however, clearly have nonergodic features. To analyze their correlations we define new, especially tailored observables which we refer to as *directed* correlators. Instead of averaging isotropically as for $C(kr)$, we now carry out the averages either only across or only along the channel in which the superscar exists similar to [23]. We thereby obtain the correlators $C^{\perp}(kr)$ and $C^{\parallel}(kr)$, respectively. In the top row of Fig. 4 the three correlators of a constructed V superscar $\Psi^{(\mathsf{V})}_{m,n}(\vec{r})$ are depicted. While the isotropic correlator $C(kr)$ follows the $J_0(kr)$ prediction up to a certain scale, the directed correlators strongly deviate from it. The results for $C^{\perp}(kr)$ and $C^{\parallel}(kr)$ show that the constructed superscar fills the channel and moves through it as a sine wave; see also Fig. 1. This information about the form of the waves, however, is washed out when averaging over all wave functions in the billiard. As the middle row of Fig. 4 shows, each of the three correlators worked out for all measured wave functions coincides with the $J_0(kr)$ prediction for chaotic systems. Hence, we may use Berry's random wave approach even though our billiard system is pseudointegrable. Importantly, we only use the two-point correlations and only go up to $kr = 8$.

We now use these observations to extract information about the superscar couplings from the measured correlators. Correlators averaged over all experimentally observed V superscars are displayed in the bottom row of Fig. 4. They are similar to, but slightly different from, those for the constructed V superscars in the top row. The difference is due to the leaking of the superscar out of the channel or, in the language of the doorway description, due to the coupling of the background states to the superscar. We thus model the measured superscars $\Psi^{(\mathsf{F})}_{\tilde{f}}(\vec{r})$ for family F as a linear combination of a constructed superscar $\Psi^{(\mathsf{F})}_{m,n}(\vec{r})$, which only contributes in the channel, and a state $\tilde{\chi}_k(\vec{r})$ which is ergodically distributed everywhere in the billiard,

$$\Psi^{(\mathsf{F})}_{\tilde{f}}(\vec{r}) = c_{\max}\Psi^{(\mathsf{F})}_{m,n}(\vec{r}) + \sqrt{1 - c^2_{\max}}\tilde{\chi}_k(\vec{r}). \qquad (7)$$

This ansatz is fully consistent with the RMT model set up above and extends it by also modeling the spatial dependence. The states describing the background should, first, have $J_0(kr)$ correlations and, second, be orthogonal to $\Psi^{(\mathsf{F})}_{m,n}(\vec{r})$. Thus, we choose the ''scarless'' plane waves

$$\tilde{\chi}_k(\vec{r}) = \frac{\chi_k(\vec{r}) - \langle\Psi^{(\mathsf{F})}_{m,n}|\chi_k\rangle\Psi^{(\mathsf{F})}_{m,n}(\vec{r})}{\sqrt{1 - \langle\Psi^{(\mathsf{F})}_{m,n}|\chi_k\rangle^2}}, \qquad (8)$$

with standard plane waves $\chi_k(\vec{r})$. The superscar contribution in the plane waves is small (but not negligible); the distribution of the overlaps $\langle\Psi^{(\mathsf{F})}_{m,n}|\chi_k\rangle$ has a standard deviation of 0.13. We convinced ourselves that the correlator of the $\tilde{\chi}_k(\vec{r})$ follows the $J_0(kr)$ prediction very closely. We work out the three correlators for the model (7). They depend on $c_{\max}$ which is, just as in the RMT model above, the coupling to the superscar doorway. By fitting to the measured superscar families we determine the couplings $c_{\max}$. The fits for the V superscar are shown in Fig. 4. The resulting $\langle c^2_{\max}\rangle$ values in Table I are close to those obtained from the RMT model. This is a nice mutual confirmation. For comparison, we also give the resulting $\Gamma^{\downarrow}$ values in Table I. Obviously, our new observables are more appropriate. This is borne out in the large standard deviation of the $\Gamma^{\downarrow}$ distribution which is, e.g., for the W superscar family, 0.8.

We conclude that our doorway interpretation yields a thorough understanding of the experimental findings. Our two new observables give deeper insight into the statistical features of the doorway mechanism as such, and it is encouraging to see how well the two analyses agree.

We thank E. Bogomolny and B. Dietz for valuable discussions. We acknowledge support from DFG (SFB 634, SFB/TR12) and from Det Svenska Vetenskapsrådet.

[1] A. Bohr and B. Mottelson, *Nuclear Structure* (Benjamin, New York, 1969), Vol. 1.
[2] V. V. Sokolov and V. Zelevinsky, Phys. Rev. C **56**, 311 (1997).
[3] H. L. Harney, A. Richter, and H. A. Weidenmüller, Rev. Mod. Phys. **58**, 607 (1986).
[4] V. Zelevinsky, Annu. Rev. Nucl. Part. Sci. **46**, 237 (1996).
[5] S. Åberg *et al.*, Phys. Lett. B **598**, 42 (2004).
[6] A. Shevchenko *et al.*, Phys. Rev. Lett. **93**, 122501 (2004).
[7] T. Guhr and H. A. Weidenmüller, Chem. Phys. **146**, 21 (1990).
[8] I. Kawata *et al.*, Phys. Rev. A **62**, 031401(R) (2000).
[9] M. S. Hussein *et al.*, Ann. Phys. (N.Y.) **284**, 178 (2000).
[10] H.-J. Stöckmann, *Quantum Chaos: An Introduction* (Cambridge University Press, Cambridge, England, 2000).
[11] E. Bogomolny and C. Schmit, Phys. Rev. Lett. **92**, 244102 (2004).
[12] E. Bogomolny *et al.*, Phys. Rev. Lett. **97**, 254102 (2006).
[13] E. J. Heller, Phys. Rev. Lett. **53**, 1515 (1984).
[14] T. Guhr, A. Müller-Groeling, and H. A. Weidenmüller, Phys. Rep. **299**, 189 (1998).
[15] M. V. Berry, J. Phys. A **10**, 2083 (1977).
[16] D. M. Brink, Doctoral thesis, Oxford University, 1955.
[17] P. Axel, Phys. Rev. **126**, 671 (1962).
[18] E. B. Bogomolny, U. Gerland, and C. Schmit, Phys. Rev. E **59**, R1315 (1999).
[19] E. Vergini, J. Phys. A **37**, 6507 (2004).
[20] N. Frazier, B. A. Brown, and V. Zelevinsky, Phys. Rev. C **54**, 1665 (1996).
[21] V. Doya *et al.*, Phys. Rev. E **65**, 056223 (2002).
[22] K. Schaadt *et al.*, Phys. Rev. E **68**, 036205 (2003).
[23] A. Bäcker and R. Schubert, J. Phys. A **35**, 539 (2002).